Visualizing the dynamics of complex spatial networks in structured fluids

S. Scherdel
Chemische Physik, TU Chemnitz, Reichenhainer Straβe 70, D-09126 Chemnitz, Germany

H. G. Schoberth
Physikalische Chemie II, Universität Bayreuth, Universitätsstraβe 30, D-95440 Bayreuth, Germany

R. Magerle[a)]
Chemische Physik, TU Chemnitz, Reichenhainer Straβe 70, D-09126 Chemnitz, Germany

(Received 19 January 2007; accepted 15 May 2007; published online 5 July 2007)

We present a data reduction and visualization approach for the microdomain dynamics in block copolymers and similar structured fluids. Microdomains are reduced to thin smooth lines with colored branching points and visualized with a tool for protein visualization. As a result the temporal evolution of large volume data sets can be perceived within seconds. This approach is demonstrated with simulation results based on the dynamic density functional theory of the ordering of microdomains in a thin film of block copolymers. As an example we discuss the dynamics at the cylinder-to-gyroid grain boundary and compare it to the epitaxial cylinder-to-gyroid phase transition predicted by Matsen [Phys. Rev. Lett. **80**, 4470 (1998)]. © *2007 American Institute of Physics*. [DOI: 10.1063/1.2747598]

I. INTRODUCTION

Block copolymers and ordered mesophases of surfactants form spatially complex structures on the nanometer scale.[1] These materials have attracted a large interest as templates for the synthesis of nanostructures of inorganic materials.[2] Furthermore interesting similarities exist to biomembranes[3] and intracellular compartments in living cells.[4] In the past decade different experimental techniques such as electron tomography[5,6] and nanotomography[7] have been developed to obtain volume images of these structures with 10 nm resolution.

At the same time advances in theory and simulation methods allow us to predict the structure and dynamics of these systems.[8] Of particular interest for the understanding of the structure formation processes is the spatial structure of individual defects and grain boundaries and their dynamics during shear flow,[9–11] structural phase transitions,[13–15] and their behavior in electric fields.[6,16–21]

The typical simulation result is the spatiotemporal evolution of the density distribution of block copolymer components within the simulated volume. The data set consists of several thousand snapshots of such density distributions (Fig. 1). Figure 1(a) shows the density distribution on the boundary of the simulated volume. The task is to also display the internal structure within the simulated volume, to do this for all time frames, and to enable the viewer to perceive the spatially complex structures as well as their temporal evolution. Because of the large number of available time frames, methods are needed which allow for a fast reception of the spatially complex dynamics. The techniques to display three-dimensional data sets either with two-dimensional projections or on stereo displays are called volume rendering.[12] The conventional approaches to visualize three-dimensional block copolymer microdomain structures are isodensity surfaces [Figs. 1(b) and 1(c)]. Because the typical volume fraction of the material is in the 30%–50% regime, meaningfull isodensity threshold values give rather dense networks which obstruct the view into the simulation box. A common way to overcome these visualization problems is to crop the volume and display only small parts of the entire structure.[22] An alternative is to display only a two-dimensional cross section through the volume data set[23] or to restrict oneself to the study of two-dimensional or quasi-two-dimensional systems.[13–15,18,21]

A direct volume rendering using an appropriate transparency map[12] is also not suitable for an easy reception and recognition of block copolymer microdomain structures in large volumes because of the rather smooth density variations. Alternative representations of microdomain structures are intermaterial dividing surfaces,[24] the reduction of microdomains to their skeleton,[25] and medial surfaces.[26]

In this work we present a method for preception of the spatially complex dynamics in block copolymers and other structured fluids. The method consists of two steps. First the microdomain structures are reduced to their minimal features: connections are represented as thin smooth lines and branching points as small spheres of different colors. The resulting network and its dynamics are visualized with a tool for protein visualization. As a result, the viewer can perceive large data streams with hundreds of volume images within seconds when displayed as an animated sequence of images (movie). As an example, we present the dynamics of a transient defect in a thin film of block copolymers simulated with dynamic density functional theory (DDFT).[27] The microdomain structures resemble the gyroid-to-cylinder transition predicted by Matsen using self-consistent field theory

[a)]Author to whom correspondence should be adressed. Electronic mail: robert.magerle@physik.tu-chemnitz.de

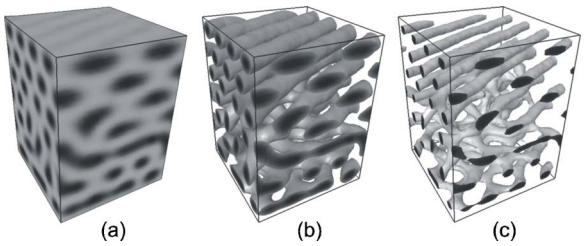

FIG. 1. Mesodyn simulation of a $A_3B_{12}A_3$ block copolymer film in a simulation box, with film thickness $H=42$, interaction parameter $\epsilon_{AB}=7.1$, surface field $\epsilon_M=6.0$, and periodic boundary conditions. The surfaces are located at the top and the bottom of the simulation box. (a) Density distribution of the A component after 1600 time steps. Dark corresponds to a high A density. (b) Corresponding isodensity surface for a threshold value $\rho_A=0.33$. The enclosed volume corresponds to the volume fraction of the A component. (c) Isodensity surface for $\rho_A=0.75$.

(SCFT).[28] Our simulation result shows the same structure and orientation of the defect, however, a different dynamics.

II. METHOD

A. Visualization

Our visualization approach is schematically shown at a detail (Fig. 2) of a much larger data set (Fig. 1). Starting from the three-dimensional (3D) density distribution of the A component we set the threshold $\rho_A=0.33$ and obtain the isosurface [Fig. 2(a)]. It encloses all pixels with density values greater than the threshold value. The result is a binarized 3D volume data set which we skeletonize in the next step.

For this, different algorithms exist which have been reviewed in Refs. 33 and 34. The algorithms differ in certain features such as robustness, thinness, invariance under isometric transformations, symmetry, efficiency, and homotopy (see, e.g., Ref. 35).

We have chosen the algorithm of Tsao and Fu[36] which is based on local connectivity and topology and is easy to implement. It iteratively removes so-called simple points until only the skeleton is left. A simple point is a border point whose deletion does not change the topology in its $3\times3\times3$ vicinity. To prevent the removal of surface or curve end points the preservation of topology is also checked in the two 3×3 vicinities of the point which are parallel to the thinning direction and to every one of the other two axes perpendicular to the thinning direction. First, the two-dimensional medial surface which consists of the centers of the maximal balls inscribed into the objects which are skeletonized is computed and subsequently in a second pass the one-dimensional medial axis. A drawback of the algorithm is its sensitivity to noise and that it removes voxels only from one particular direction in each pass. Because of this, it is sensitive to the predetermined order of the different directions and hence not rotational invariant. The resulting skeleton is shown in Fig. 2(b).

Our implementation of the algorithm of Tsao and Fu does not account for the periodic boundary conditions of the original data set and introduces artifacts in about 5 pixels wide zone at the boundary. We have solved this problem by enlarging the data set by periodic continuation of 16 pixels in each direction and cropping the resulting skeleton to the original size of the data set.

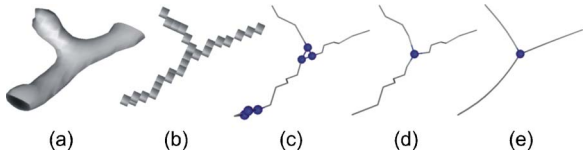

FIG. 2. (Color online) Illustration of our data reduction and visualization technique. (a) A small piece of isodensity surface displaying a branching cylinder. (b) Medial axis obtained by applying the thinning algorithm of Tsao and Fu. (Ref. 37). (c) Visualization of the data shown in (b) as a stick and ball model. Kinks reflect the discrete points of the medial axis. Balls mark branching points with the color coding of the number of branches. (d) Same as (c) after removal of artifacts, such as clusters of balls. (e) Same as (d) with the branches approximated by a cubic smoothing spline.

The next step is to transform the skeleton to a stick and ball model [Fig. 2(c)]. To this end we use the data format of the protein database[37] (PDB) which is a standard for filing of protein structures which can be considered as complex network structures.

Due to the noise of ρ_A and the discreteness of the data different artifacts exist. The most frequent artifacts are short (1–2 grid units long) protrusions and clusters of threefold branching points at positions where the cylinders branch. Furthermore the connecting lines are irregular. In a first pruning step the short protrusions and clusters [such as in Fig. 2(c)] are identified and removed [Fig. 2(d)] by comparing them with an empiric catalog of artifacts. The pruning is done in the following way:

(I) Assign to each point (voxel) of the skeleton a value corresponding to its number of neighbors
(II) Find a point with at least three neighbors
(III) Inspect the values of the neighbors of this point

(1) If there is a neighbor with value of 1 (one voxel protrusion)
  (a) Delete this neighboring point
  (b) Correct the value of the primary point

(2) If there are neighbors with value of 2
  (a) Check if one of them is connected to another neighbor of the primary point
  (b) If there is such a pair then delete the neighbor with value of 2 and correct the values of the points neighboring to the deleted point

(3) If there are at least two neighbors with a higher value than 2: Search for two neighbors which are connected to each other (they form a triangle). If such a triangle is found
  (a) Place a new point in the center of the triangle
  (b) Delete the old triangle and add connections to the new point
  (c) Set the values of the new point and correct the values of its neighbors

(4) Repeat step 3 until no triangles are found

With these pruning steps also more complex examples can be reduced. For illustration of the pruning algorithm see supplementary data.[38]

At this step the branching points and end points are colored according to the number of branches. Then the irregular connecting lines are smoothed by cubic smoothing splines [Fig. 2(e)]. As we used the PDB format the result can be visualized in 3D with various software tools, for instance PYMOL.[39] A particular feature is its ability to view the 3D data set in stereo mode and anaglyph views. From the series of anaglyph views we have produced movie 1 (see supplementary data[38]).

B. MESODYN computer simulation

For demonstrating our visualization approach we have used the result of a MESODYN simulation[29] similar as in Ref. 27 where the structure formation in a thin film of cylinder forming block copolymer melt is modeled. $A_3B_{12}A_3$ block copolymers are modeled as Gaussian chains with different beads A and B. A Gaussian kernel characterized by ϵ_{AB} is used to model the bead-bead interaction potential. The film interfaces were treated as masks (M) with a corresponding bead-mask interaction parameter $\epsilon_M=\epsilon_{AM}-\epsilon_{BM}$. For the spatiotemporal evolution of bead densities $\rho_i(r,t)$ the complete free energy functional $F[\rho_i]$ and the chemical potenials $\mu_i=\partial F[\rho_i]/\partial\rho_i$ are used. The Langevin diffusion equation is solved numerically starting from homogeneous densities. An appropriate noise is added to the dynamics. For details on the simulation method see Ref. 30.

MESODYN simulations predict correctly the equilibrium structure[27,29–32] and the microdomain dynamics[13] in thin films of block copolymers. In order to demonstrate our new visualization approach we have chosen a simulation run of a thick film with film thickness of $H=42$ grid units and interaction parameters $\epsilon_{AB}=7.1$ and $\epsilon_M=6.0$ (both in kJ/mol). For details of the parametrization and the resulting equilibrium structures see Ref. 27. The particular simulation run used in this work is a typical result. Different noise and another initialization of the random number generator would cause another dynamics but the same final equilibrium structure.

III. RESULTS

As an example to demonstrate our visualization approach we have modeled the structure formation process in a thin film of block copolymer. The simulation result is the density distribution of the two components A and B as a function of space and time. The isodensity surfaces show the change of the microdomain structure from the initially homogeneous distribution to the equilibrium structure of hexagonally ordered cylinders. The rather thick microdomains obstruct the view into the inner parts of the simulated volume [Figs. 1(b) and 1(c)]. This makes it difficult to observe the details of structural rearrangement processes. With our data reduction the isosurface is transformed to a network of thin smooth lines with branching points colored by their connectivity order (Fig. 3 and movie 2 in the supplementary data[38]). Compiling the series of images into a stereo view or anaglyph movie and playing it in a fast mode make it easy to percept the block copolymer dynamics over some 10 000 time steps within seconds. The coding of branching points makes it easier to orient within the structure and to recognize characteristic structures and defects.

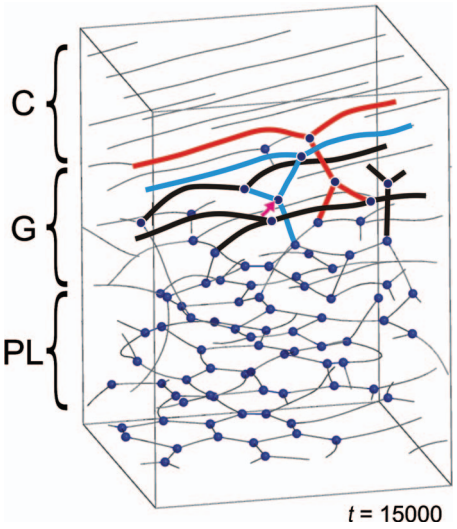

FIG. 3. (Color) Reduced representation of the network of A cylinders in a thin film of $A_3B_{12}A_3$ block copolymers, calculated from an isosurface with threshold value $\rho_A=0.33$ for 15 000 time steps. The thin lines do not obstruct the view into the simulation box. The complex 3D network structure is much better perceivable in the anaglyph movie 1 (see supplementary data, Ref. 39). Three different structures are visible in the simulation box: in the upper third hexagonally orderd cylinders (C), in the middle a gyroid like network (G), and in the lower third layers of perforated lamellae (PL). Our visualization technique allows us to see and follow the 3D dynamics of the network. A characteristic detail of the structure at the cylinder-to-gyroid boundary is marked with thick lines and displayed in Fig. 4(a) along with its further dynamics.

Starting from a homogeneous distribution the two components first microphase separate and form microdomains with no long-range order. This process is finished after about 200 time steps. The next step is the much slower ordering process of microdomains.

In the first phase (200–3000 time steps) the microdomains orient parallel in the vicinity of surfaces and form a layer of perforated lamellae at each surface. In the middle of the film the microdomains remain disordered. In the following the order propagates towards the center of the film. This result is similar to the simulation results of Ref. 40 who have first studied with MESODYN simulations the surface induced ordering process in a lamella forming system. We study a cylinder forming system close to the gyroid and perforated lamella phases.[27]

The ordering process towards hexagonally ordered cylinders involves transient phases such as the gyroid and perforated lamella phases. In addition our particular simulation is complicated by a spontaneous symmetry break into differently ordered phases which we attribute to the fact that the involved phases are energetically similar. At the upper surface cylinders are formed already after 9000 time steps, whereas at the lower surface the perforated lamella remains. In the middle a disordered network of microdomains exists which we consider as gyroidlike because of the large number of threefold connections. The layer of the cylinders next to the upper surface acts as a nucleus for the equilibrium phase

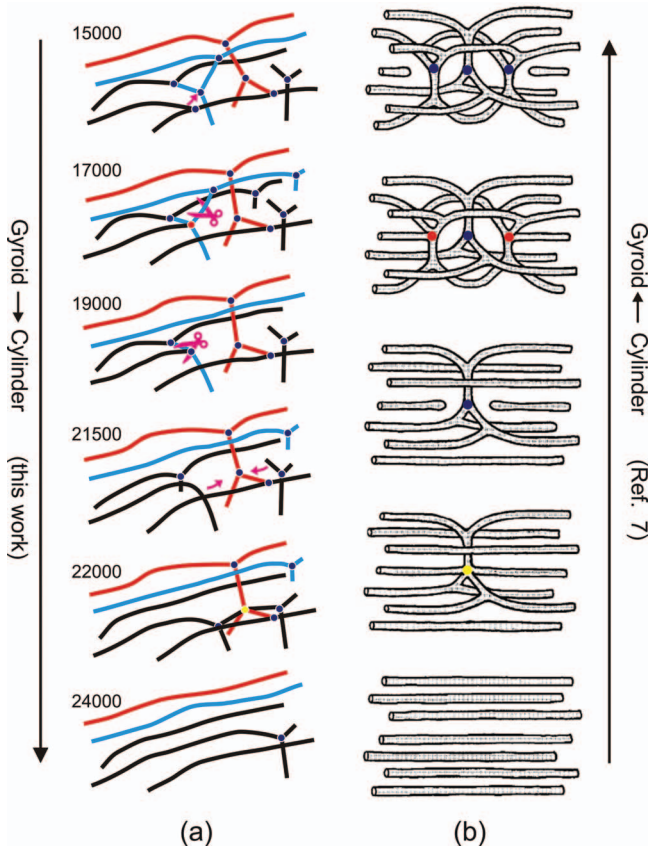

FIG. 4. (Color) (a) Sequence of microdomain structures during the gyroid-to-cylinder transition observed in this work. The corresponding time steps are displayed in the figure. The arrow marks a moving connection, the scissors mark a breaking connection. (b) Sequence of structures during the cylinder-to-gyroid transition predicted by Matsen (Ref. 29). The color coding of branching points is the same as in Fig. 3. Adopted from Ref. 29; ©1998 American Physical Society).

of hexagonally ordered cylinders. Starting from this layer the phase grows towards the lower surface. Close to the end (at 29 000 time steps) almost the whole structure has transformed to hexagonally ordered cylinders except for a few defects and two rings of a perforated lamella in the vicinity of the bottom surface. At 34 000 time steps the equilibrium structure of hexagonally ordered cylinders is reached.

The situation at 15 000 time steps is shown in Fig. 3. The color coding of branching points reveals that the network structure is mainly built up from threefold connections. Fourfold and fivefold connections are seldom and very short living. This indicates that these defects are energetically very unfavorable.

The elementary step of the structural transformation process turns out to be the stepwise breakup and formation of connections between microdomains. An interesting example for this is the microdomain dynamics at the cylinder-to-gyroid grain boundary. The corresponding microdomains are marked in Fig. 3 with thick lines. The color coding is introduced to distinguish the different cylinders in the 2D projection. The cylinders orient in layers parallel to the upper surface. At the boundary to the gyroidlike phase the threefold branching points which bridge cylinders in neighboring layers are characteristic for the gyroid structure. In Fig. 4(a) the temporal evolution of this structural feature is shown. The transformation proceeds via stepwise breaking and forming of connections of microdomains. For instance, one of the black cylinders shown in Fig. 4(a) moves along the purple arrow by first breaking up in the vicinity of the threefold connections ($t=17\,000$) and then connecting to the neighboring threefold connection and forming a fourfold branching at $t=17\,750$. At a later stage this fourfold branching breaks up stepwise starting at the position marked by the purple scissors. During the transformation process a fourfold and a fivefold connection appear but only for a very short period of time.

This example shows how with our visualization technique an interesting process can be identified in the center of the simulation box. It is important to keep in mind that the original data set is the dynamics of a density distribution. Therefore we now return to a representation of the data which is better suited to display the details of a continuous density distribution. Figure 5 shows the density distribution in the plane defined by the cylinders marked in Fig. 3 with thick black lines together with the isosurface of these cylinders. The dynamics is best seen in the corresponding movie (movie 2 in the supplementary data[38]). The sequence of snapshots shown in Fig. 5 illustrates the stepwise breaking and forming of connections between cylinders described above and shown in Fig. 4. In addition to the skeleton of the cylinders this representation reveals details of the density distribution such as the thinning of breaking connections, the thickening of open ends, and density modulations along the microdomains which belong to the gyroidlike structures. The structures at the intermediate steps resemble characteristic structural features predicted by Matsen who has studied theoretically the gyroid-to-cylinder transition with self-consistent field theory [Fig. 4(b)].[29]

IV. DISCUSSION

A. Visualization method

We have demonstrated our method on block copolymer micordomain structures forming cylinders, perforated lamellae, and gyroidlike structures. These structures represent a large part of the mesophases in block copolymers and sur-

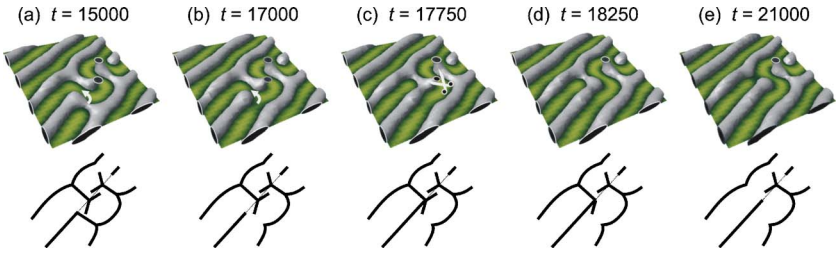

FIG. 5. (Color online) [(a)–(e)] Snapshots of movie 2 (see supplementary data, Ref. 39) showing the dynamics of the A density in the plane defined by the thick black lines shown in Figs. 3 and 4(a). Light (dark) green corresponds to a low (high) ρ_A density. In addition the isodensity surfaces (gray) are shown.

factant based structured fluids. Hence, our approach should be straightforward applicable on experimental data and simulation results of such systems with, if any, only slight changes or extensions of the empiric lookup table. Our visualization approach can also be used to visualize experimental data of the microdomain dynamics at the surface of thin films of block copolymers similar as in Refs. 13, 14, and 41. For the visualization of lamellae appropriate representations need to be found which do not obstruct the view into the volume. As we intended only a proof of principle we implemented our algorithm in MATLAB (MathWorks, Inc.; Version 7.0.1.24704) and did not emphasize a fast implementation. With an optimized implementation of the algorithm an online visualization simultaneously with the simulation run or the experimental data acquisition might be achieved.

B. MESODYN computer simulation

The stepwise breaking and forming of connections corresponds nicely with the experiments by Knoll *et al.*[13] who studied the cylinder-to-perforated-lamella transition in a thin film. The simulations shown in their work also predict the stepwise process. In our present work we have used the same model but with slightly different interaction parameters ϵ_{AB} and ϵ_M.

We now return to the mechanism of the gyroid-to-cylinder transformation process and compare the sequence of structures with that predicted by Matsen.[28] Our result [Fig. 4(a)] shows this transition at the boundary to the cylinder phase. At $t=15\,000$ two threefold branching points are located next to each other and both are not connected to its neighboring cylindrical microdomain. At $t=17\,000$ the left threefold branching has transformed to a fourfold branching by connecting to its neighboring cylindrical microdomains. The details of the transformation process are described with Figs. 4(a) and 5.

In the following the fourfold branching breaks up step by step until at $t=21\,500$ only one threefold branching point remains. It transforms to a fivefold branching (at $t=22\,000$) by connecting simultaneously to its neighboring microdomains. Finally, this fivefold branching breaks up stepwise until at $t=24\,000$ this region has completely transformed to hexagonally ordered cylinders. The intermediate steps are shown in movie 1.

Matsen has predicted very similar structures for the cylinder-to-gyroid and the gyroid-to-cylinder transitions. We observe the same sequence of structures as Matsen has predicted for the cylinder-to-gyroid transition [Fig. 4(b)] but in the opposite temporal order. An important difference between the two models is that we observe the microdomain dynamics at the cylinder-to-gyroid grain boundary where the cylinder phase grows at the expense of the gyroid phase. In contrast, Matsen's SCFT calculation assumes the transition between the cylinder phase and the gyroid phase to occur simultaneously throughout the entire sample such that the morphology remains periodic. His SCFT uses the same type of functional for the free energy as our DDFT model, and he determines the lowest energy pathway connecting the local minima of the cylinder and gyroid mesophases. Figure 4(b) does not represent an actual SCFT calculation but provides results from it and shows a typical sequence of forming and breaking of connections. In our DDFT model no *a priori* assumptions about the structures are made. The local densities diffuse spontaneously along local gradients of the chemical potentials of the two components.

It is very interesting that despite the different approaches the same sequence of structures is predicted. We believe that this is caused by the fact that in both models the same type of energy functional is used. Since in DDFT no assumptions are made about the structure and since no translational symmetry exists in the z direction because of the cylinder-to-gyroid grain boundary and the presence of the surface, it is not astonishing that the details of the intermediate steps predicted by DDFT differ from Matsen's results.

Furthermore, we like to emphasize that the discussed pathway of the structural transformation process is the result of one particular simulation run. Another initialization of the random number generator, different noise, and slightly different other parameters (such as film thickness, the size of the simulation box, ϵ_{AB}, and ϵ_M) would probably cause another dynamics but the same final equilibrium structure. More simulation runs would be needed to determine whether the observed dynamics of the cylinder-to-gyroid grain boundary occurs frequently.

V. SUMMARY

We have demonstrated an approach for visualizing the 3D structure and dynamics of large data sets of block copolymers. The method is also applicable to other types of structured fluids such as surfactant phases. The constantly increasing computer power allows us to simulate large volumes over long time periods. This shifts the challenge from calculating to grasping and interpretation of the huge amount of data. Movies prepared with our visualization method allow us to perceive the dynamics of spatially complex network structures within a minute.

ACKNOWLEDGMENTS

This work was supported by the Deutsche Forschungsgemeinschaft (SFB 481) and the VolkswagenStiftung. The authors also thank M. W. Matsen for clarifying his results on the cylinder-to-gyroid transition.

[1] I. W. Hamley, *The Physics of Block Copolymers* (Oxford University Press, Oxford, 1998).
[2] C. Park, J. Yoon, and E. L. Thomas, Polymer **44**, 6725 (2003).
[3] K. Katsov, M. Müller, and M. Schick, Biophys. J. **87**, 3277 (2004); **90**, 915 (2006).
[4] S. Hyde, S. Andersson, K. Larsson, Z. Blum, T. Landh, S. Lidin, and B. W. Ninham, *The Language of Shape* (Elsevier Science, Amsterdam, 1997).
[5] H. Jinnai, Y. Nishikawa, R. J. Spontak, S. D. Smith, D. A. Agard, and T. Hashimoto, Phys. Rev. Lett. **84**, 518 (2000).
[6] T. Xu, A. V. Zvelindovsky, G. J. A. Sevink, K. S. Lyakhova, H. Jinnai, and T. P. Russell, Macromolecules **38**, 10788 (2005).
[7] R. Magerle, Phys. Rev. Lett. **85**, 2749 (2000).
[8] For a review, see, G. H. Fredrickson, V. Ganesan, and F. Drolet, Macromolecules **25**, 16 (2002).
[9] A. V. Zvelindovsky, G. J. A. Sevink, B. A. C. van Vlimmeren, N. M. Maurits, and J. G. E. M. Fraaije, Phys. Rev. E **57**, R4879 (1998).
[10] A. V. Zvelindovsky and G. J. A. Sevink, Europhys. Lett. **62**, 370 (2003).

[11] A. V. Zvelindovsky, G. J. A. Sevink, and J. G. E. M. Fraaije, Phys. Rev. E **62**, R3063 (2000).
[12] B. Lichtenbelt, R. Crane, and S. Naqvi, *Introduction to Volume Rendering* (Prentice-Hall PTR, Upper Saddle River, NJ, 1998).
[13] A. Knoll, K. S. Lyakhova, A. Horvat, G. Krausch, G. J. A. Sevink, A. V. Zvelindovsky, and R. Magerle, Nat. Mater. **3**, 886 (2004).
[14] L. Tsarkova, A. Horvat, G. Krausch, A. V. Zvelindovsky, G. J. A. Sevink, and R. Magerle, Langmuir **22**, 8089 (2006).
[15] K. S. Lyakhova, A. Horvat, A. V. Zvelindovsky, and G. J. A. Sevink, Langmuir **22**, 5848 (2006).
[16] T. Xu, A. V. Zvelindovsky, G. J. A. Sevink, O. Gang, B. Ocko, Y. Zhu, S. P. Gido, and T. P. Russell, Macromolecules **37**, 6980 (2004).
[17] I. W. Hamley, V. Castelletto, O. O. Mykhaylyk, and Z. Yang, Langmuir **20**, 10785 (2004).
[18] K. Schmidt, A. Böker, H. Zettl *et al.*, Langmuir **21**, 11974 (2005).
[19] K. S. Lyakhova, A. V. Zvelindovsky, and G. J. A. Sevink, Macromolecules **39**, 3024 (2006).
[20] K. Schmidt, H. G. Schoberth, F. Schubert, H. Hänsel, F. Fischer, T. M. Weiss, G. J. A. Sevink, A. V. Zvelindovsky, A. Böker, and G. Krausch, Soft Matter **3**, 448 (2007).
[21] A. V. Zvelindovsky and G. J. A. Sevink, Phys. Rev. Lett. **90**, 049601 (2003); A. V. Kyrylyuk, A. V. Zvelindovsky, G. J. A. Sevink, and J. G. E. M. Fraaije, Macromolecules **35**, 508 (2002).
[22] See, e.g., Fig. 10 in Ref. 6; Figs. 6 and 7 in Ref. 10; and Figs. 3, 6, 9, and 11 in Ref. 11.
[23] See, e.g., Figs. 1, 3, and 4 in Ref. 9.
[24] D. Hoffman, Nature (London) **384**, 28 (1996).
[25] See, e.g., Figs. 16, 17, and 18 in M. E. Vigild, K. Almdal, K. Mortensen, I. W. Hamley, J. P. A. Fairclough, and A. J. Ryan, Macromolecules **31**, 5702 (1998).
[26] G. E. Schröder-Turk, A. Fogden, and S. T. Hyde, Eur. Phys. J. B **54**, 509 (2007).
[27] A. Horvat, K. S. Lyakhova, G. J. A. Sevink, A. V. Zvelindowvsky, and R. Magerle, J. Chem. Phys. **120**, 1117 (2004).
[28] M. W. Matsen, Phys. Rev. Lett. **80**, 4470 (1998).
[29] J. G. E. M. Fraaije, J. Chem. Phys. **99**, 9202 (1993); J. G. E. M. Fraaije, B. A. C. van Vlimmeren, N. M. Maurits, M. Postma, O. A. Evers, C. Hoffmann, P. Altevogt, and G. Goldbeck-Wood, *ibid.* **106**, 4260 (1997); G. J. A. Sevink, A. V. Zvelindovsky, B. A. C. van Vlimmeren, N. M. Maurits, and J. G. E. M. Fraaije, *ibid.* **110**, 2250 (1999).
[30] A. Knoll, A. Horvat, K. S. Lyakhova, G. Krausch, G. J. A. Sevink, A. V. Zvelindovsky, and R. Magerle, Phys. Rev. Lett. **89**, 035501 (2002).
[31] A. Knoll, R. Magerle, and G. Krausch, J. Chem. Phys. **120**, 1115 (2004).
[32] K. S. Lyakhova, A. Horvat, R. Magerle, G. J. A. Sevink, and A. V. Zvelindovsky, J. Chem. Phys. **120**, 1127 (2004).
[33] L. Lam, S.-W. Lee, and C. Y. Suen, IEEE Trans. Pattern Anal. Mach. Intell. **14**, 869 (1992).
[34] M. W. Jones, J. A. Bærentzen, and M. Sramek, IEEE Trans. Vis. Comput. Graph. **12**, 581 (2006).
[35] T. Grigorishin, G. Abdel-Hamid, and Y.-H. Yang, Pattern Analysis and Applications **1**, 163 (1998).
[36] Y. F. Tsao and K. S. Fu, Comput. Graph. Image Process. **17**, 315 (1981).
[37] F. C. Bernstein, T. F. Koetzle, G. J. B. Williams, E. F. Meyer, Jr., M. D. Brice, J. R. Rodgers, O. Kennard, T. Shimanouchi, and M. Tasumi, J. Mol. Biol. **112**, 535 (1977); H. M. Berman, J. Westbrook, Z. Feng, G. Gilliland, T. N. Bhat, H. Weissig, I. N. Shindyalov, and P. E. Bourne, Nucleic Acids Res. **28**, 235 (2000); http://www.pdb.org/
[38] See EPAPS Document No. E-JCPSA6-127-004725 for illustration of the pruning algorithm and two movies of the microdomain dynamics corresponding to Figs. 3 and 5, respectively. This document can be reached through a direct link in the online article's HTML reference section or via the EPAPS homepage (http://www.aip.org/pubservs/epaps.html).
[39] W. L. DeLano, PYMOL, DeLano Scientific, San Carlos, CA, 2002; http://www.pymol.org.
[40] G. J. A. Sevink and A. V. Zvelindovsky, J. Chem. Phys. **121**, 3864 (2004).
[41] L. Tsarkova, A. Knoll, and R. Magerle, Nano Lett. **6**, 1574 (2006).